ICES CIEM

International Council for the Exploration of the Sea
Conseil International pour l'Exploration de la Mer

Accounting for spatio-temporal distribution changes in size-structured abundance estimates for a data-limited stock of *Raja clavata*

Timo Michael Staeudle [1,*], Bram Parmentier[2,3], Jan Jaap Poos [1,4]

[1]Aquaculture and Fisheries Group, Wageningen University and Research, 6700 AH Wageningen, The Netherlands
[2]Wildlife Ecology and Conservation Group, Wageningen University and Research, 6708 PB Wageningen, The Netherlands
[3]NIOZ, the Royal Netherlands Institute for Sea Research, 1790 AB Den Burg (Texel), The Netherlands
[4]Wageningen Marine Research, Wageningen University and Research, 1970 AB IJmuiden, The Netherlands

*Corresponding author. Aquaculture and Fisheries Group, Wageningen University and Research, 6700 AH Wageningen, The Netherlands. E-mail: timo.staeudle@wur.nl

Abstract

Vulnerability of elasmobranchs to fishing and declines in populations over the last decades have prompted calls for improved fisheries management and conservation efforts. The *Raja clavata* (Thornback ray) population in the Greater North Sea ecoregion is a population that has historically shown marked declines with increasing industrialized fishing, while a lack of robust catch data of commercial fisheries hampers assessment of population abundance. Using fisheries-independent survey catch data haul-by-haul surface area estimates, we employ integrated-nested Laplace approximation to estimate total and size-class abundances of *R. clavata*. By accounting for spatio-temporal changes in the population, size selectivity between survey gears, and minimizing bias from partially overlapping survey areas, we demonstrate major changes in the abundance and distribution over the past three decades. Notably, increases of abundance in the Eastern English Channel and south-eastern North Sea result in an overall increase in the abundance and biomass of the population. Our findings expand understanding of the spatio-temporal dynamics and exploitation of this data-limited stock, emphasizing the potential for improved population abundance estimates to inform future stock assessments.

Keywords: spatio-temporal models; integrated nested laplace approximation; elasmobranch; thornback ray; greater North Sea

Introduction

The impacts of the world's fisheries on the marine environment are substantial, affecting species that are used for food or feed, and on species that are caught as bycatch (Kelleher 2005). Among these bycatches are elasmobranchs that are particularly vulnerable to mortality caused by fishing (Musick et al. 2000, Gallagher et al. 2012, Worm et al. 2024). This vulnerability to fishing can be contributed to life-history traits commonly associated with low rates of population growth, such as slow somatic growth, low fecundity, and slow maturation (Walker and Hislop 1998, Stevens et al. 2000, Ellis et al. 2008). Being meso- and top predators, declines in elasmobranch populations transform the structure and function of marine communities through trophic cascades, competitive release, and species replacement (Stevens et al. 2000, Baum and Worm 2009). Therefore, declines in elasmobranch populations over the last decades have resulted in calls for increasing conservation efforts (Dulvy et al. 2008, Stein et al. 2018, Sherman et al. 2022).

Raja clavata (Thornback ray) is an elasmobranch species inhabiting the Northeast Atlantic that showed marked declines in abundance in the North Sea and English Eastern Channel, managed as the North Sea, Skagerrak, Kattegat, and Eastern English Channel stock, between the 1960s and the 1990s (Walker and Heessen 1996, Engelhard et al. 2015), following the introduction of mechanised bottom trawling (Engelhard 2008). This decline of *R. clavata* coincided with a progres-

sive reduction of a historically widespread distribution that spanned across the entire southern North Sea in the 1900s to a distribution reduced to the Greater Thames Estuary and Humber Estuary in the 1980s (Walker and Heessen 1996, Sguotti et al. 2016). Its population has since been concentrated in the south-western North Sea with relative abundance trends derived from research vessel survey catches suggesting an increase in abundance (ICES 2021).

Meanwhile, a lack of robust catch data from commercial fisheries hinders the assessment of population abundance and exploitation pressure from stock assessments, relying on these catches (Aarts and Poos 2009, Sampson 2014, Cook 2019). The mandatory reporting of landings by species for Rajidae in the greater North Sea ecoregion only started in 2009 (Amelot et al. 2021). Moreover, species misidentification of commercial catches has been common because of morphological similarities within the genus Raja (Thys et al. 2023). As a result, no species-specific commercial catch estimates were available prior to 2007. Stock assessments based on unreliable long time series of catches are thus uncertain (ICES 2017). Moreover, a common total allowable catch for ray species, implemented in 1999 by the European Commission, encourages the discarding of non-valuable rays over valuable rays, hampering estimation of total catches from shore-based landings (ICES 2017, Amelot et al. 2021).

In contrast, data from research vessel surveys can inform long-term trends in local population abundances. Species

identification on board of research vessels is done by trained observers. Hence, species misidentification is expected to occur substantially less frequently compared to fisheries catch data. The research vessel surveys, however, often have limited geographic ranges in which they sample (Bogaards et al. 2009). Within these surveys, variances in individual samples are often high, owing to spatial and temporal heterogeneity in abundance (Pinto et al. 2019, Alglave et al. 2022). This heterogeneity is caused by species migration under the influence of ontogenetic niche shifts, seasonal spawning migration, local differences in mortality, aggregation behaviour, and individual responses of animals to changes in the environment (Dulvy et al. 2017, McInturf et al. 2023). Models that aim to provide population-level abundance estimates must thus be able to account for spatiotemporal variability that affects species abundance and patterns (Thorson and Minto 2015).

Integrated-nested Laplace approximation (INLA), proposed by Rue et al. (2009), is a powerful method for analysing variability in species abundance, through spatial and temporal correlation structure in latent variables. The importance of accounting for spatial variability in marine populations has long been recognized in marine ecology and marine resources management (Goethel and Cadrin 2021). It is thus no surprise that INLA is gaining popularity to address issues where spatial heterogeneity plays a strong role (Pinto et al. 2019). It has been used to identify fish nurseries (Paradinas et al. 2015), identify best fishing-suitable areas (Paradinas et al. 2016), explore predator–prey and competitor species habitat overlap (Sadykova et al. 2017), and to predict the occurrence of *Mobula mobular* from incidental catches (Lezama-Ochoa et al. 2020). Generally, the spatial distributions are estimated from incidence, rather than abundance (Pennino et al. 2013, 2016, Pinto et al. 2019).

Here, we use INLA to estimate total and size-structured abundance of *Raja clavata* in ICES Subarea 4 and division 7.d, using surface area (SA) estimates of fisheries-independent research vessel survey data, explicitly accounting for spatial and temporal changes in the population. By using an INLA model that is explicitly size structured and uses count data rather than incidences, we aim to obtain abundance estimates, and distinguish between effects of recruitment and mortality. We combine long-term survey data from the database of trawl surveys (DATRAS), spanning more than 30 years, allowing for differences in the size selectivity between gears used in the different surveys.

Methods

Survey data
Research-vessel catch data for the North Sea and Eastern English Channel was obtained from ICES database on trawl surveys (DATRAS), hosted by the International Council for the Exploration of the Sea (ICES; ICES 2023b). The data were downloaded in the exchange format for the International Bottom Trawl Survey (NS-IBTS) for Quarters 1 and 3, the Beam Trawl Survey (NS-BTS) for Quarter 3, and the Channel Groundfish Survey (FR-CGFS) for Quarter 4. The exchange format in DATRAS included two relevant datasets, haul records and length records of catches. The latter included species identification codes, counts of catch per length, geographic location of haul, time of haul, haul duration in minutes, haul length in meters, and gear width estimates.

While the NS-IBTS surveys have covered the North Sea since 1977, the FR-CGFS has covered the Eastern English Channel only since 1988. Hence, we have chosen 1988 as the first year of the analyses. Throughout the study period, the North Sea was continuously covered by the NS-IBTS and NS-BTS, while coverage of the English Channel increased over time with the addition of BTS hauls since 1990, and NS-IBTS hauls since 2007. The last year of the analyses is 2023. A full overview of the haul locations per year and survey is given in Figs S1–S3.

All valid hauls were retained from the haul records, while data for *R. clavata* (WoRMS AphiaID: 105883) was selected by only using catches with valid length measurement. For each haul, catch in counts per haul was calculated, aggregated into three length classes based on commercial landing size and length-at-maturity. The threshold for commercial landing size was defined as 50 cm, with individuals <50 cm being classified as unexploited, and individuals ≥50 cm being classified as exploited. The threshold for maturity classification for *R. clavata* was defined as 71 cm, with individuals <71 cm being classified as immature, and individuals ≥71 cm being classified as mature. This threshold was based on estimated lengths at 50% maturity in the North Sea, being 68 cm for males (Walker 1999) and 74 cm for females (McCully et al. 2012). This resulted in three size class classifications of individuals being categorized as size class 1, unexploited-immature individuals of size <50 cm, size class 2, exploited-immature individuals of size interval [50 cm, 71 cm), and size class 3, exploited-mature individuals of size ≥71 cm.

To account for the differences in sampling between surveys that use different gears, the fished SA for each haul was calculated. The fished SA was based on wingspread times trawled distance for NS-IBTS and FR-CGFS and total beam width times trawled distance for NS-BTS. Missing SAs for the NS-IBTS were inferred from a linear relationship between SA and haul duration. The intercept of this relationship was set to zero, and its slope was estimated using a regression analysis of the available data for SA and haul duration. Missing trawled distance for the NS-BTS were inferred from a linear relationship between trawled distance and haul duration. The intercept of this relationship was set to zero, and its slope was estimated using a regression analysis of trawled distance and haul duration.

The gear of the FR-CGFS survey was changed between 2014 and 2015, with limited information about the wingspread prior to 2014. The wingspread prior to 2014 was set to 10.34 m, based on Auber et al. (2015). Missing wingspreads in 2015 were set to be equal to average wingspread in the period 2016–2023.

Environmental variables
Habitat, substrate, and depth potentially affect the spatial distribution of *R. clavata* (Sguotti et al. 2016, Wright et al. 2020). Therefore, European Nature Information System habitat types and substrate information from EUSeaMap 2021 Broad-Scale Predictive Habitat Map for Europe (Vasquez et al. 2021) were obtained (Fig. S4). Habitat and substrate information for each haul was extracted by intersection of haul shoot position with polygons of substrate (Table S1) and habitat (Table S2).

Depth data were obtained from the European Marine Observation and Data Network (EMODnet). For the greater

North Sea ecoregion, this depth data is spread over four tiles: D4, D5, E4, and E5. These tiles were combined, and the spatial resolution was upscaled to 1×1 km. Depth information for each haul was obtained by intersecting geographic haul location using shooting position and the depth grid. The maximum depth at which *R. clavata* was caught was 165 m. Hence, hauls deeper than 165 m (1.1%) were excluded from further analysis to improve model fitting.

Modelling catches of *R. clavata* maturity classes

The model building followed a hierarchical Bayesian framework approach using stochastic partial differential equations (SPDE) in "R-INLA" package (https://www.r-inla.org; Rue et al. 2009, Lindgren et al. 2011, Lindgren and Rue 2015) in R (R Core Team 2024), allowing for direct interpretation of spatial and temporal dependencies in the data. The mixed-effects model was defined as follows:

$$C_{it} \sim \text{NB}(\mu_{it}, \, k),$$
$$E(C_{it}) = \mu_{it},$$
$$\text{var}(C_{it}) = \mu_{it} + \frac{\mu_{it}^2}{k},$$
$$\log(\mu_{it}) = I + \text{Survey} + \text{Size class} + \text{Survey} \times \text{Size class}$$
$$+ \text{offset}(\log(\text{SA})) + \alpha_{tm} + \beta_{dm} + \upsilon_{it},$$
$$\alpha_{tm} = \alpha_{t-1,m} + \eta_{t,m}, \quad \eta_{tm} = N\left(0, \, \frac{1}{\rho_{\eta_{t,m}}}\right),$$
$$\beta_{dm} = \beta_{d-1,m} + \eta_{d,m}, \quad \eta_{dm} = N\left(0, \, \frac{1}{\rho_{\eta_{d,m}}}\right),$$
$$\upsilon_{it} = \rho \times \upsilon_{i,t-1} + \upsilon_{it},$$
$$\upsilon_{it} \sim \text{GMRF}(0, \, \Sigma),$$

where C_{it} represents catch in numbers of individuals per haul location i in year (t), assuming negative binomial distribution. The negative binomial model has an estimated mean (μ_{it}) and estimated shape parameter (k). The mean was modelled using an intercept I and multiple covariates: Survey has three levels, one for each of the surveys, to estimate differences among surveys, given all other relevant factors such as location, year, and size class. Three size classes were used in the model: with size class 1 represented by $m = 1$, size class 2 by $m = 2$, and size class 3 by $m = 3$. The interaction between surveys and size classes is also included to account for the fact that surveys may have varying gear efficiencies across size classes. The offset term incorporates the log of the SA for each haul. Because of the log link in the model, the estimated mean count increases linearly with SA. Habitat or substrate covariates were added as fixed effects to test for their influence on catches.

Three random walks describe trends in mean count over discrete years for the three size classes. This allows the model to fit different trends for size classes over time, with estimates for year effect α_{tm} changing between years by η_{tm}, modelled as a normal distribution with mean zero and precision $\rho_{\eta_{t,m}}$. Likewise, three random walks describe trends for discrete 1-m depth steps (d) by β_{dm} with the error term η_{dm} modelled as a normal distribution with mean zero and precision $\rho_{\eta_{d,m}}$. Finally, there is a spatio-temporal component of the model defined as υ_{it}, the combination of a spatially autoregressive gaussian random field (υ_{it}), a Gaussian Markov random field (GMRF) with mean 0 and covariance matrix Σ. Changes in the GMRF occur over time, using an autoregressive function, where ρ determines how much previous years affect subsequent years. The temporal autocorrelation was modelled as an AR1 process with nine equally spaced temporal knots from 1988 to 2023, to reduce computational costs (Banerjee 2004, Jona Lasinio et al. 2013).

The GMRF can be approximated using a SPDE in the INLA-SPDE approach (Rue et al. 2009). Using INLA-SPDE relies on discretizing space by defining a mesh that creates an artificial set of neighbours over the study area, allowing for estimation of the spatial autocorrelation between observations (Rue et al. 2009, Van Niekerk et al. 2023). A stationary solution of the SPDE has a Matérn covariance function that gives the spatial correlation (Zuur et al. 2017), using two parameters, a local precision parameter τ and a scale parameter κ (Rue et al. 2009, Zuur et al. 2017). The marginal variance σ_u^2 and range ρ are functions of these parameters, with variance σ_u^2 being $1/(4 \times \pi \times \tau^2 \times \kappa^2)$ and range ρ being $\sqrt{8}/\kappa$ in our application that is using two-dimensional space. The required mesh was generated using Delaunay triangulation (Berg et al. 2008) with boundaries that were generated in several steps. First, a non-convex boundary polygon was created from all observations, with an extension radius that was equal to 2% of the approximate diameter of the observation set. This non-convex boundary polygon was then restricted to be contained within the Greater North Sea to prevent overlap with landmasses. This boundary polygon was then used to create a mesh with an inner and outer boundary. The inner boundary was equal to the boundary polygon. The outer boundary extended this boundary polygon by our initial guess of the range of spatial autocorrelation, being 130 km, based on visual inspection of the data.

For the inner mesh, the largest allowed triangle edge length was set to 26 km, being 20% of our initial guess for spatial autocorrelation. For the outer mesh, the largest allowed triangle edge length was three times larger. This resulted in a fine scale inner mesh comprising of the study area, with a coarser outer mesh to avoid edge effects in our estimates. The minimum allowed distance between points (cut-off) was set to 20 km. This resulted in a mesh with 1407 nodes (Fig. S5).

Models of increasing complexity were compared through Watanabe–Akaike information criterion (WAIC) and mean logarithmic condition predictive ordination (LCPO) (Table 1). Models 1–4 did not include spatial or temporal correlations, models 5–8 included spatial correlation, and models 9–12 included spatial and temporal correlations. WAIC measures the compromise between fit and parsimony, LCPO (Roos and Held 2011) assesses the predictive power of the model as a "leave one out" cross-validation index (Pennino et al. 2013, Lezama-Ochoa et al. 2020). Lower WAIC and LCPO suggest better model performance.

Priors, starting values, and model fits

Default diffuse INLA priors were used for the intercept, fixed effects, and random effects. For the intercept, this means a normally distributed prior with mean and precision equal to 0. The fixed effects are assigned normally distributed priors with mean equal to 0 and precision equal to 0.001. For $\log(\kappa)$, a normally distributed prior was used, based on the approximate diameter of the mesh, such that the distribution mean was equal to $\log(\sqrt{8}/(0.2 \times \text{mesh diameter}))$, and precision was equal to 0.1. For $\log(\tau)$, a normally distributed prior was used, based on the prior mean for κ, such that the distribution

Table 1. Summary of model structure.

Model	Added fixed effects	Depth RW	WAIC	LCPO
Non-spatial				
1			71 968	35 400
2		+	67 417	33 811
3	Habitat	+	66 047	32 742
4	Substrate	+	65 470	32 850
Spatial				
5			55 479	27 499
6		+	54 214	27 034
7	Habitat	+	54 209	27 036
8	Substrate	+	54 181	27 020
Spatio-temporal				
9			52 692	26 479
10		**+**	**51 743**	**26 001**
11	Habitat	+	51 744	26 041
12	Substrate	+	51 869	26 031

All models included fixed effects for the interaction between survey and size-class, and a random walk for year, for each size class. The model with the lowest WAIC and mean LCPO is indicated in bold. Plus signs (+) indicate the presence of a random walk effect for depth.

mean was equal to $\log(\sqrt{1/4\pi} \times (\text{prior mean } \kappa)^2)$, and precision equal to 0.1.

Model convergence was evaluated using the eigenvalues of the Hessian matrix, and convergence was declared if all eigenvalues were positive. For complex models where default starting values did not yield model convergence, starting values from previously fitted simpler models were provided and refitted, using the inla.rerun() function, until a successful fit was found.

Model predictions and abundance estimations

The model with the lowest WAIC and LCPO was used to make predictions and to generate annual spatial distributions of abundance estimates. To estimate medians and 95% credible intervals (CI) for model predictions and abundances, 1000 samples were drawn from an approximated posterior of the fitted model. For each sample, count estimates were generated for cells on a regular grid of 5 km^2 cell size, for each size class and year. The boundaries of the prediction grid were set by the interior mesh that was used when fitting the model. At each grid location, depth was determined from the depth dataset.

The area used for generating the abundance estimates was set to the surface of the cells, so that predictions equalled expected counts in each cell. Catchability of surveys was accounted for by multiplying expected counts in each cell with the inverse of two efficiency multipliers, following Walker et al. (2017). The first efficiency multiplier was set to 0.95 for the largest mean length-at-age, representing species found predominantly on the seabed with flat body shapes (Walker et al. 2017). The second efficiency multiplier consisted of size class specific catchability for the highest gear efficiency of the average length per size class, based on species specific gear efficiencies for *R. clavata* obtained from Walker et al. (2017) (Fig. S6; Table S3).

To generate biomass estimates from the abundance estimates per size class, a weight-length equation was used to estimate mean weight per size class:

$$W_m = aL_m{}^b,$$

where W_m was the weight for size m in grams, L_m was the length of the size in cm. The a and b parameters were obtained from McCully et al. (2012) by averaging across sex. This resulted in an estimate of a being 0.0054 and b being 3.0465.

The average weight for each of the three size classes was then calculated as the average weight within the size class, weighted by the catches per size.

Summing the estimated counts and biomass over the entire grid provided estimations of total population abundance ($A_{t,m}$) and total biomass ($B_{t,m}$), for each year t and size class m. In turn, these were summed to obtain the total population abundance and biomass for each year.

The total exploited-unexploited ratio (EUR) was calculated for each year from the predicted population abundance for each year and size class:

$$\text{EUR}_t = A_{t,m=2,3}/A_{t,m=1}.$$

This EUR_t was then smoothed by applying a moving average. The window for this average was equal to the 8-year generation time of *R. clavata*, averaged over the two sexes (Walker 1999). This moving average reduces noise likely due to recruitment and reveals long-term trends of the EUR as a proxy for mortality. Summarizing posterior estimates over the grid cells contained within Roundfish Areas (RFA) provided estimations of total population abundance for each year and size class per RFA with 95% credible intervals.

Results

Survey data

The entire dataset contained 34 620 hauls for the three surveys, of which 4428 contained catches of *R. clavata*. With 20 761 hauls, the NS-IBTS had the largest number of hauls in the dataset, followed by the BTS with 10 862 hauls. Size class 1 was caught in 3250 hauls, size class 2 was caught in 2155 hauls, and size class 3 was caught in 944 hauls.

Model evaluations

Accounting for depth as a random effect reduced WAIC and LCPO within non-spatial, spatial, and spatio-temporal models (Table 1). Explicitly accounting for spatial and spatio-temporal variation in the models further reduced WAIC and LCPO (Table 1). The addition of either habitat or substrate as covariates did not improve the WAIC or LCPO when spatio-temporal variation was explicitly accounted for (Table 1). Model 10 demonstrated the lowest WAIC and LCPO (Table

Table 2. Numerical summary of the marginal posterior distribution of fixed effects.

Parameter	Mean	SD	Q0.025	Q0.975
Intercept	− 3.252	0.511	− 4.253	− 2.250
Size class 2	− 1.001	0.219	− 1.431	− 0.571
Size class 3	− 2.542	0.247	− 3.026	− 2.057
Survey: FR-CGFS	− 0.985	0.069	− 1.121	− 0.849
Survey: NS-IBTS	− 0.623	0.069	− 0.758	− 0.488
Survey: FR-CGFS × size class 2	1.371	0.089	1.196	1.546
Survey: FR-CGFS × size class 3	2.466	0.118	2.235	2.696
Survey: NS-IBTS × size class 2	0.300	0.094	0.116	0.484
Survey: NS-IBTS × size class 3	0.816	0.128	0.565	1.068

For each parameter, the mean, SD, and 95% (Q0.025–Q0.975) credible intervals are provided. The intercept included the NS-BTS survey, size class 1.
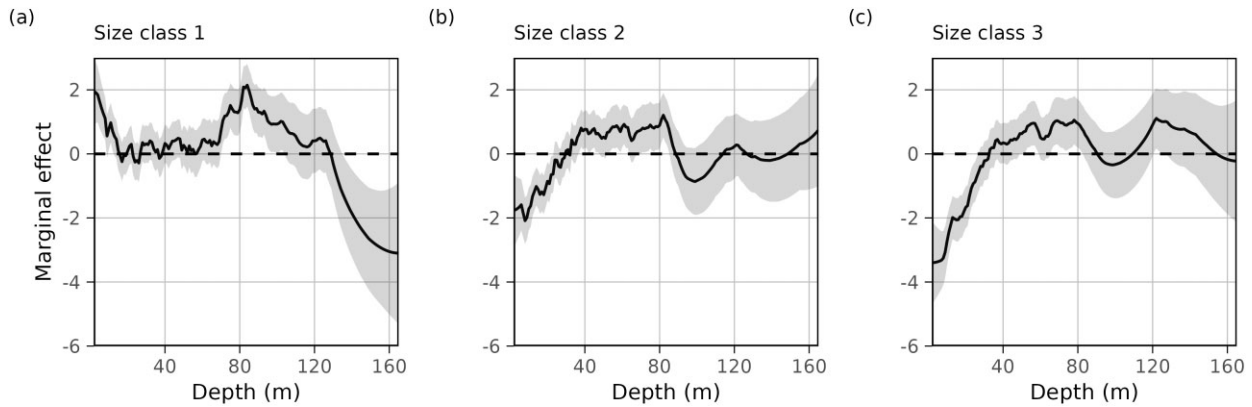
Figure 1. Marginal effect size of depth as random walk for the three size classes with 95% credible intervals: (a) size class 1 (<50 cm); (b) size class 2 ([50 cm, 71 cm)); and (c) size class 3 (≥71 cm).

1) and was therefore chosen as the best model to perform predictions.

Model fit with predictions

The interaction between survey and size class was interpreted to result from differences in gear efficiency among the three surveys. The highest gear efficiency for size class 1 was estimated for the NS-BTS survey (in Intercept; Table 2). The two other surveys showed significantly lower gear efficiency for this size class (Table 2). The parameter estimates for size classes 2 and 3 were negative, suggesting a decrease in catches with increase size class for the NS-BTS (Table 2). The interaction between survey and size class pointed to relative higher gear efficiencies for size classes 2 and 3, relative to size class 1, when comparing FR-CGFS and NS-IBTS to NS-BTS (Table 2). As a result, the NS-BTS appeared to have the highest gear efficiency for size class 1, while the FR-CGFS showed the highest gear efficiency for size classes 2 and 3.

The marginal effect for depth differed substantially among the three size classes. For the smallest size class, the marginal effect decreased with depth in the first 20 m, then increased approaching 90 m, followed by a decrease (Fig. 1). For the intermediate size class, the estimated abundances increased with depth at depths below 50 m. This effect of increasing abundance with depth at depths below 50 m was more pronounced in the largest size class (Fig. 1).

The spatial correlation in the data was estimated to have a range of ∼120 km (95% CI: 106–136 km) (Fig. 2), following from an estimated K of 0.023 (SD = 0.001; Table 3) in the Matérn covariance function. The autoregressive parameter value ρ for the temporal effect was estimated to be 0.857
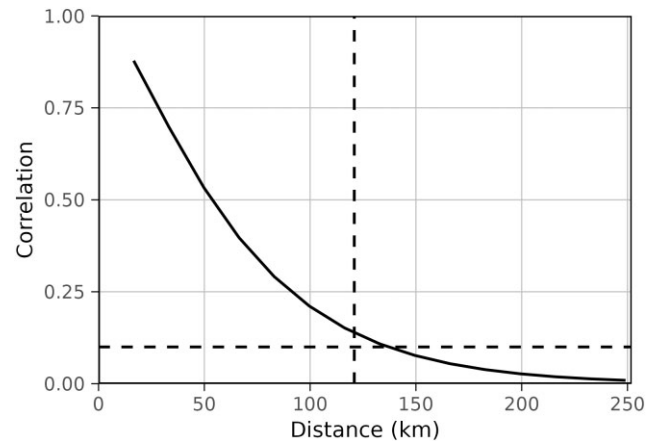

Figure 2. The Matérn correlation function (solid line) describes the correlation between locations in the SPDE model in relation to their distance to each other. The vertical dashed line indicates the estimated range, at which the correlation is ∼0.1 (horizontal dashed line).

(SD = 0.015; Table 3), indicating a strong correlation between the nine equally spaced temporal knots of the model. The resulting posterior mean (Fig. S7) and standard deviations (SDs) (Fig. S8) for the estimated spatial field are provided in the supplementary materials.

Spatial abundance predictions

The spatial distribution for all size classes of *R. clavata* changed noticeably over the period from 1988 to 2023. From 1988 a distinct hotspot in abundance was observed in the

Table 3. Numerical summary of the marginal posterior distribution of the hyperparameters.

Parameter	Mean	SD	Q0.025	Q0.975
k	0.341	0.006	0.329	0.354
$\rho_{\eta_{t,m=1}}$	1.649	0.467	0.914	2.78
$\rho_{\eta_{t,m=2}}$	4.235	1.281	2.232	7.354
$\rho_{\eta_{t,m=3}}$	6.416	1.573	3.863	10.088
$\rho_{\eta_{d,m=1}}$	0.586	0.127	0.375	0.881
$\rho_{\eta_{d,m=2}}$	0.696	0.175	0.414	1.112
$\rho_{\eta_{d,m=3}}$	0.843	0.233	0.475	1.410
ρ	0.857	0.015	0.825	0.884
κ	0.023	0.001	0.021	0.027
τ	3.542	0.199	3.166	3.949

For each parameter, the mean, SD and 95% (Q0.025-Q0.975) credible intervals are provided.

Western North Sea near the Wash and Humber estuaries on the east coast of England, while at the same time, a hotspot off the Greater Thames Estuary expanded (Fig. 3). Abundances in the Eastern English Channel increased in the early 2000s (Figs 3 and 4). Meanwhile, a distinct and persistent area of relatively low abundance was observed in the north-east of the Eastern English Channel from 1988 to 2023, located southwest from the Strait of Dover (Fig. 3). An overall reduction of abundance was observed across the Northern North Sea, whereas increasing abundances were observed in the southeastern parts of the North Sea since 2008 (Fig. 3).

A closer look at the median predicted abundance of size classes of *R. clavata* revealed different abundance trends across RFAs (RFAs 1–7 and 10). The abundances in RFAs 2, 3, 5, 6, and 10 all surpassed their respective size-class specific pre-2000 abundance baselines at some point in time (Fig.
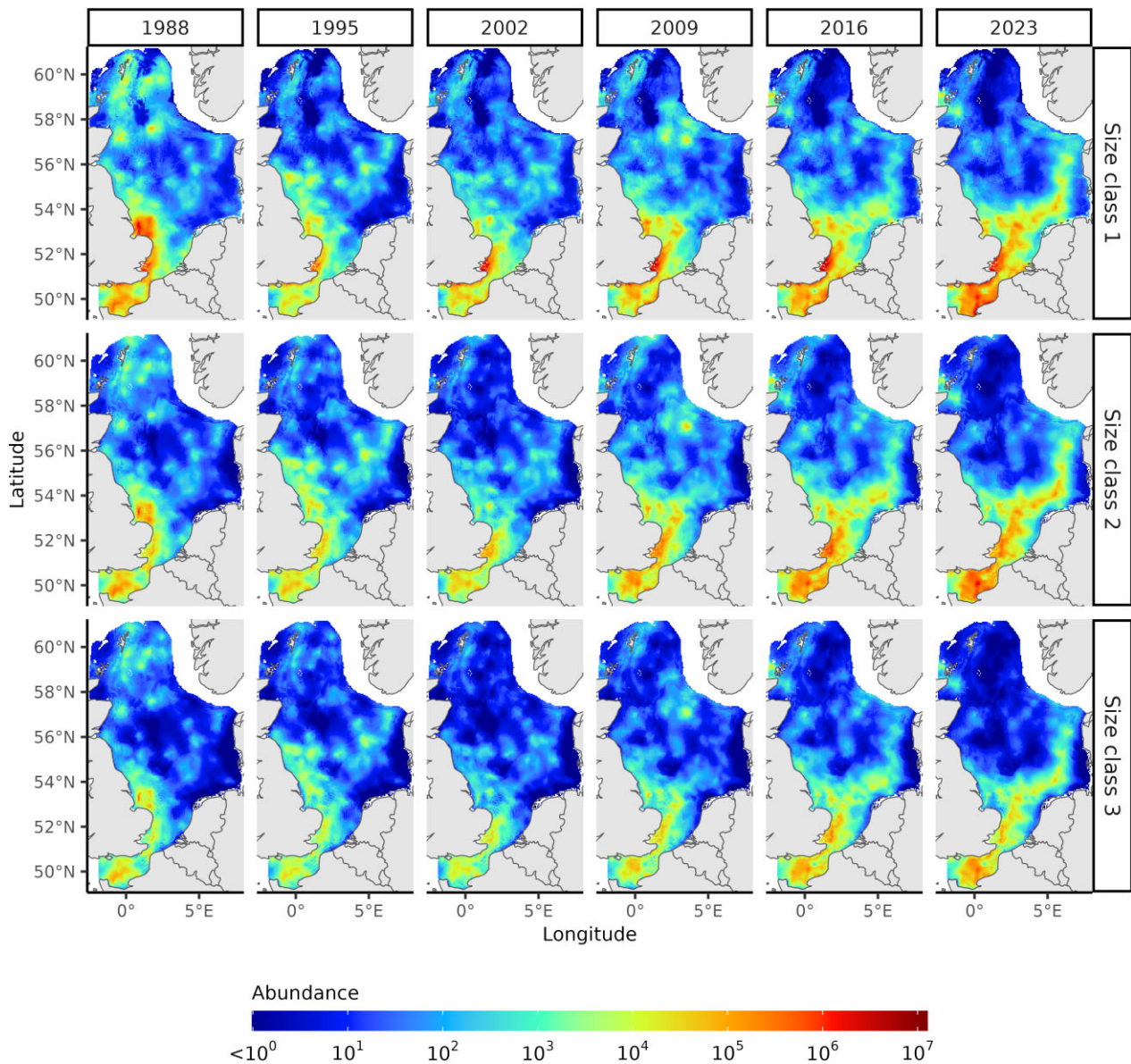
Figure 3. Predicted median abundance (in number of individuals) per 25 km^2, for *R. clavata* in the Greater North Sea study area from 1988 to 2023, for size class 1 (<50 cm), size class 2 ([50 cm, 71 cm)), and size class 3 (≥71 cm).
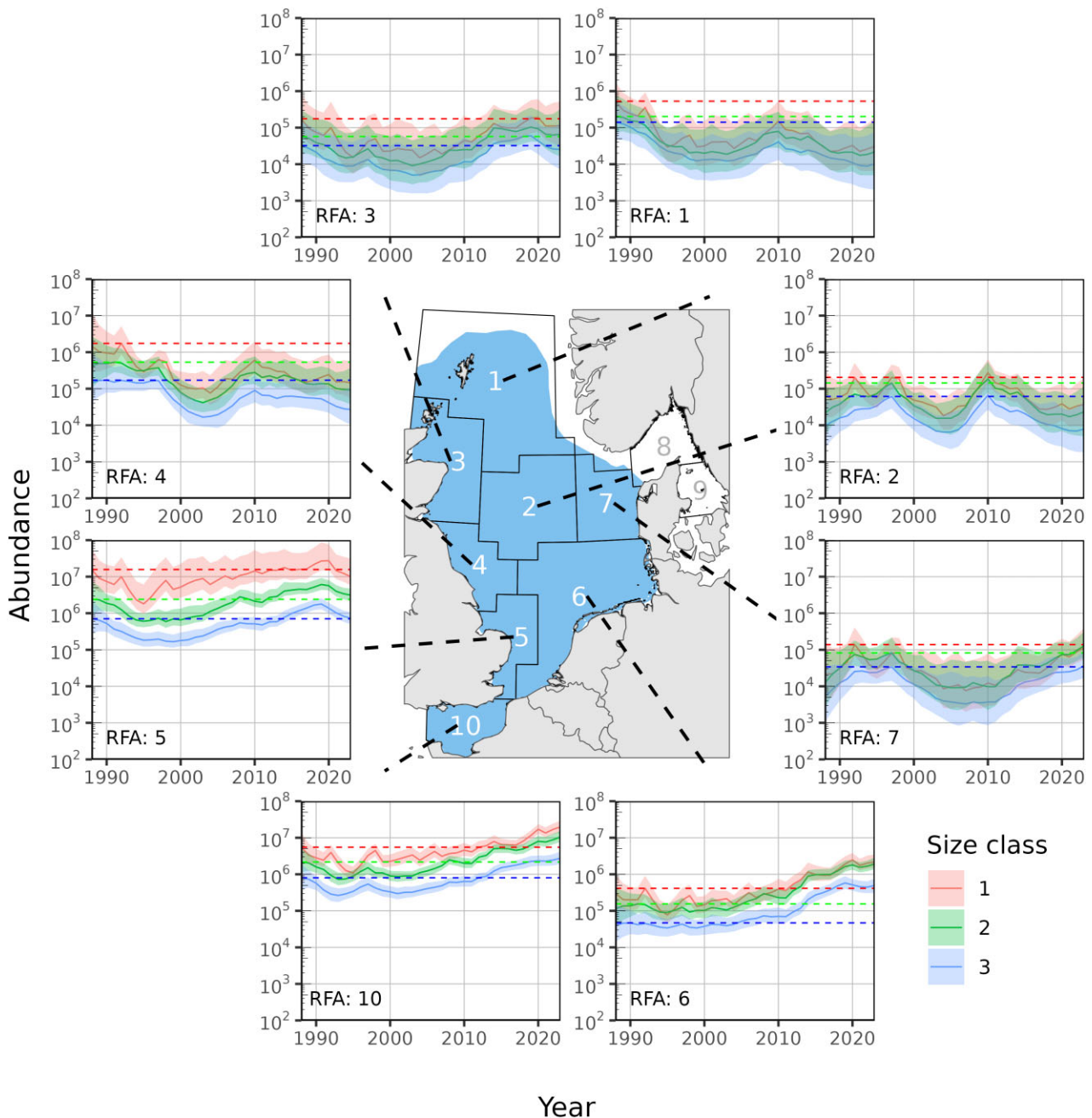
Figure 4. Predicted abundance (in number of individuals) of size classes of *R. clavata* from 1988 to 2023 for RFA 1–7 and 10, with 95% credible intervals and pre-2000 abundance peak baselines (dashed line) for size class 1, size class 2, and size class 3. The blue polygon indicates the area used for abundance predictions. Note that *y*-axes are log-scaled.

4). The increase in abundance was clearest in RFA 6 and 10. There, abundances stayed above the pre-2000 abundance baselines across all three size classes after 2013. Abundances in RFA 1–4 appeared to be fluctuating without trend or decreasing across all size classes (Fig. 4). Abundances for all size classes in RFA 7 appeared to follow recovering trends since the late 2000s, with size classes being close to their respective pre-2000 baseline by 2023 (Fig. 4).

In 2023, the greatest abundance across all three size classes of rays was found in RFA 10 with 19.67 million (95% CI: 13.83–29.17 million) for size class 1, 10.47 million (95% CI: 7.63–15.49 million) for size class 2, and 2.74 million (95% CI: 1.93–4.18 million) for size class 3 (Fig. 4).

Total abundance and biomass predictions

Total abundance for the three size classes initially decreased from 1988 onwards, followed by an increase that started in 1996 for size class 1 and in the early 2000s for size classes 2 and 3 (Fig. 5).

Size class 1 was the largest size class in the population during the entire study period. For this size class, the lowest abundance was observed in 1995, being ∼3.64 million individuals (95% CI: 2.27–8.09 million). Since 1996, abundance steadily increased, with the highest abundance being estimated in 2020 at 51.46 million individuals (95% CI: 34.45–107.79 million; Fig. 5).
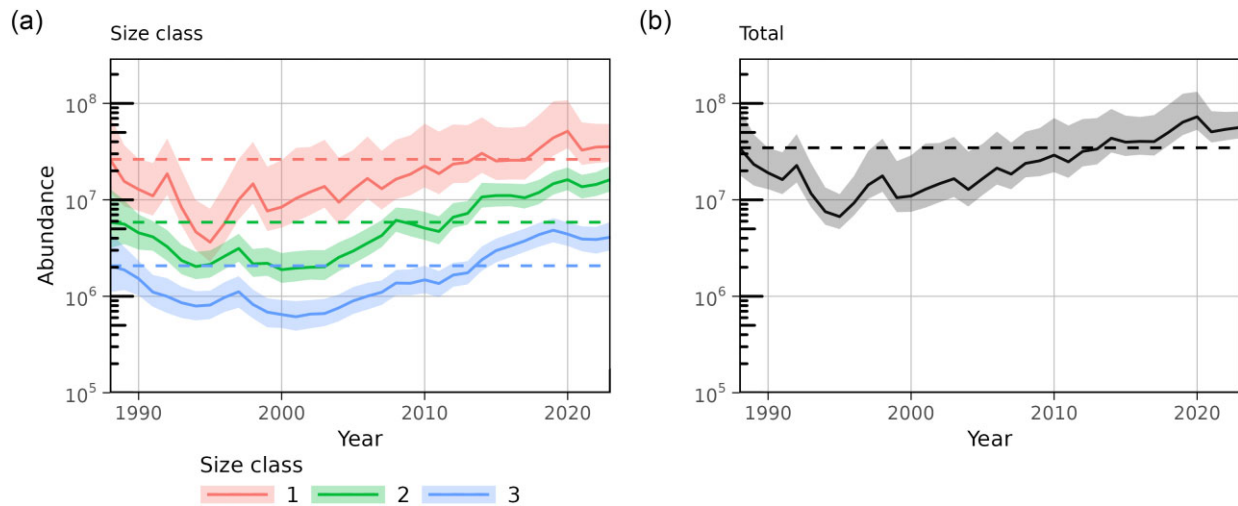
(a)

Size class

(b)

Total

Size class

Figure 5. Median predicted abundance (in number of individuals) with 95% credible intervals of size classes (a) and total (b) of *R. clavata* for the Greater North Sea study area. Pre-2000 peak abundance prediction baselines for each size class are indicated as dashed horizontal lines. Note that *y*-axes are log-scaled.
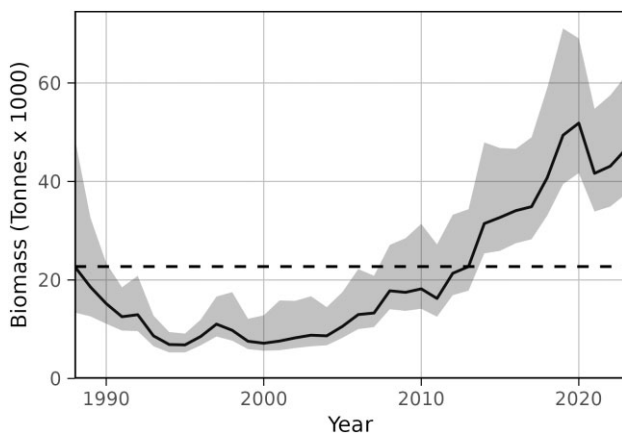

Figure 6. Median predicted biomass of *R. clavata* for the Greater North Sea study area, with 95% credible intervals and pre-2000 peak biomass prediction baselines (dashed line).

Figure 7. Median ratio of predicted abundances (in number of individuals) of exploited (≥50 cm: size classes 2 and 3) over unexploited (<50 cm: size class 1) (EUR) size classes with 95% credible intervals, and the moving average of EUR with an 8-year time span and 95% credible intervals. The pre-2000 peak of the 8-year moving average is indicated by the dashed green line.

Size classes 2 and 3 were similar in abundance throughout the study period, with minima at 1.89 million individuals (95% CI: 1.38–2.81 million) for size class 2, and 0.61 million individuals (95% CI: 0.44–0.89 million) for size class 3. Both minima occurred in the early 2000s. Both size classes increased in abundance until 2015, after which size class 2 fluctuated between 10 and 20 million and size class 3 between 3 and 5 million individuals. The abundance of size class 3, representing the adult population, was ~4.10 million individuals in 2023 (95% CI: 3.00–5.90). Combining the size classes, the total abundance peaked in 2020 at 72.63 million individuals (95% CI: 53.20–132.08 million; Fig. 5).

While the trend in total population abundance was dominated by the trend in abundance of size class 1 (Fig. 5), the trend in total population biomass was dominated by size classes 2 and 3 (Fig. S9). Median biomass decreased from 1988 to the lowest biomass level at 6.8 thousand tonnes (95% CI: 5.3–9.1) in 1995, followed by a clear upward trend in predicted biomass from 2005 onwards (Fig. 6). The median biomass peaked in 2020 at 51.9 thousand tonnes (95% CI:
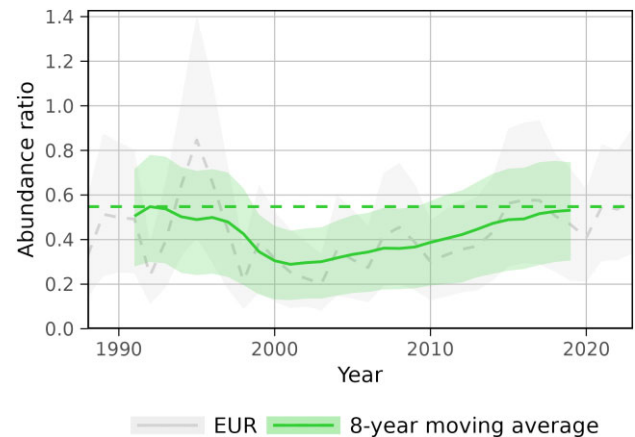
41.7–69.1; Fig. 6). Median biomass was estimated in 2023 at 46.6 thousand tonnes (95% CI: 37.5–61.5; Fig. 6).

The 8-year moving average in exploited over unexploited ratio (MA8_EUR) showed a declining trend in the pre-2000s, followed by an increasing trend since the 2000s (Fig. 7). The lowest MA8_EUR was observed in 2001 at 0.29 (95% CI: 0.13–0.44; Fig. 7). The largest MA8_EUR since 2000 was estimated for 2019 at 0.53 (95% CI: 0.31–0.75), approximately equal to the pre-2000 baseline in 1992 (Fig. 7).

Discussion

This study provides spatially explicit temporal trends in abundance for multiple size classes and multiple research vessel surveys. Spatio-temporal correlation structures in catches are accounted for using an autoregressive spatial random field, implemented in INLA (Rue et al. 2009). The results provide evidence of major changes in the abundance and distribution

of *R. clavata* in the Greater North Sea ecoregion over the past three decades. The abundances in the Eastern English Channel and south-eastern North Sea have increased, leading to an overall increase in the abundance and biomass of the population. Meanwhile, increase in the ratio of exploited over unexploited individuals over the last two decades suggests that mortality in the adult population has decreased. Our findings contribute to the understanding of the spatio-temporal dynamics and exploitation of this data-limited stock. They demonstrate the potential for achieving improved population abundance estimates for size-classes of interest by combining survey data from partially overlapping areas. They help to inform future stock assessments of stocks that are data limited. The approach we followed requires good research vessel survey data, ideally accompanied by estimates for gear efficiency derived from data-rich stocks for species with similar characteristics.

Abundance, distribution, and size composition

The difference in depth preferences observed for the three size classes suggests ontogenetic niche shifts with respect to depth. Smaller individuals were observed in shallower waters (<20 m), while larger-size classes preferred deeper waters. Nursery areas for elasmobranchs are often found in shallower waters, with migration cycles of adults between feeding grounds and mating grounds (Rousset 1990, Walker et al. 1997). This has also been observed for rays in the North Sea, where tagging data have shown that reproductively active adults migrated into shallow water (<20 m) (Hunter et al. 2005, 2006), where egg-laying takes place (Holden 1975). Large individuals were observed at depths down to 165 m. This is in contrast to populations of *R. clavata* in the Azores that occur down to 250 m depth (Santos et al. 2021).

The model results indicate an increase in abundance and biomass in the last two decades, following a decrease. This trend was previously described in incidence patterns of catches from UK research-vessel surveys (Sguotti et al. 2016), and biomass estimations from population models based on the same research-vessel surveys used in this study (Amelot et al. 2021). The decrease coincided with a progressive contraction in spatial distribution in the southern North Sea from 1902 to 2013: from a historical widespread distribution across the entire southern North Sea, the population distribution contracted to areas off the UK southeast coast in the 1980s (Sguotti et al. 2016).

The recent increase in abundance was spatially heterogeneous. The largest contributions to abundance increase come from the Eastern English Channel and south-eastern North Sea. The former area harbours the highest abundances across all size classes in 2023. Meanwhile, most areas in the north-western part of the North Sea show no sign of recent abundance increase. Whereas previously important abundance hotpots close to the Wash and Humber estuaries off the UK coast have declined (Fig. 3).

The origin of the individuals fuelling the abundance increase observed in Eastern English Channel and south-eastern North Sea is unknown. The increase could be caused by increases in locally distinct populations, e.g. because of a reduction of mortality or by migration of individuals from adjacent areas of high abundance, like the Thames estuary, as hypothesized by Walker and Heessen (1996). Migration studies using tags and genetic studies could shed light on the mechanisms

at play. Previous tagging data showed a strong site-fidelity of individuals in the Thames estuary during the egg-laying season, suggesting that repopulation through migration would be unlikely (Hunter et al. 2005). However, genetic population differentiation within the southern North Sea and Eastern English Channel is weak, suggesting a high degree of population mixing in these areas (Chevolot et al. 2006).

Meanwhile, the size composition of the population has changed, as can be observed from trends in the ratio of exploited ($\geq$50 cm) over unexploited (<50 cm) size classes in the predicted abundances. This is indicative of changes in recruitment and mortality rates over the last three decades. The smallest size class, with individuals below the marketable size, is likely dominated by individuals of ages 2 and 3 (Bellodi et al. 2024). The increase in the smallest size class could be indicative of an increase in recruitment, reduced growth, or reduced mortality of the smaller sizes. Meanwhile, the ratio of exploited over unexploited individuals in the population has been increasing since the early 2000s (Fig. 7). We hypothesize that this increase could be caused by a decrease in mortality of marketable size classes across the population in the Greater North Sea, in line with reductions in fishing effort in the North Sea. An alternative hypothesis for this increase in ratio could be an increase in growth of the population.

Applications

The size-dependent abundance trends provide the opportunity to account for trends in population abundance and mortality independent of fisheries catch data. However, the method can also be used to generate spatially aggregated "tuning" indices for surplus production stock assessment models (Pedersen and Berg 2017, Winker et al. 2018), or delay-difference models (Fournier and Doonan 1987). These stock assessment models perform best when using a single tuning series covering the entire stock (Kraak et al. 2009).

Combining data from multiple sources, such as fishery-dependent and independent data sets, across varying spatial sampling scales are increasingly being leveraged to inform species distribution modelling both outside (Fletcher et al. 2019, Moriarty et al. 2020, Alglave et al. 2022) and within an INLA approach (Pinto et al. 2019, Paradinas et al. 2023). In this study, catch data from multiple surveys that only partially overlap are combined while allowing for gradual changes in size-specific population abundance over time for a data-limited stock. This provides a potential reduction in biases that arise from partially overlapping series of surveys while providing size-specific abundance and biomass estimates for stock assessments.

The biomass estimates from the INLA model presented here follow similar trends to those estimated from surplus-production models (Amelot et al. 2021, ICES 2023a). However, the absolute biomass estimates from the INLA model are lower. The peak estimate of ~51.8 thousand tonnes in 2020 from the model presented here is lower than those estimated by Amelot et al. (2021) and by an ICES expert group (ICES 2023a). Amelot et al. (2021) estimated the biomass in 2018 to be ~80 thousand tonnes, and the ICES expert group (ICES 2023a) estimated the biomass in 2021 to be ~70 thousand tonnes. Spatio-temporal models may be biased in scale of estimated abundances (Thorson et al. 2021). Our method generates biomass predictions for survey and gear combinations with the highest gear efficiency, combined with gear efficiency

estimates from closely related species for which stock assessments are available. The difference between the estimates from the model presented here and the surplus production models needs further study. The biomass trends from our INLA model could be used as tuning index in surplus production models (Pedersen and Berg 2017, Winker et al. 2018). Biomass estimates derived from these models rely heavily on estimates of total fisheries removals from the population. These estimates are notoriously difficult for stocks for which there is limited commercial interest and where species identification is difficult. A strong belief in the correctness of the biomass estimates used as tuning index over the estimated fisheries removals could be expressed by setting a strong prior on the catchability of this tuning index being equal to 1 (Winker et al. 2018).

Challenges and future research

Given the focus on spatial correlation in our study, the mesh design that allowed the estimation of spatio-temporal correlation in our data is of crucial importance. Appropriate mesh design is currently an active field of research (Bakka et al. 2018, Righetto et al. 2020, Dambly et al. 2023). While there are no formal procedures to specify an optimal mesh, some guidelines exist (Zuur et al. 2017, Righetto et al. 2020). A common understanding is that the finer the mesh, the more accurate the Gaussian, at the expense of computational costs (Blangiardo et al. 2013). Although it has been demonstrated that spatial predictions become broader and less detailed with increasing mesh coarseness, indicating that coarser mesh density affects the level of accuracy in the predictions of spatial intensity, care has to be taken with finer meshes as they can lead to overfitting, and even large outer extensions of the mesh may not completely resolve issues with boundary effects (Dambly et al. 2023). One possible extension of study could be to have a barrier mesh that would prevent any spatial correlation to cross-land masses (Bakka et al. 2018). This problem of crossing land masses is probably negligible in our case, given the limited SA of island, the overall shape of our study area, and the migration ecology of the modelled species. However, the correlation estimates near the narrow boundary between the southern North Sea and the Eastern English Channel would probably improve with a barrier mesh.

The prediction could be extended to a multi-species approach by including additional catch data for the other species per haul, integrating a species covariate in the model to simultaneously predict catches of multiple ray species in the area. This would allow comparing changes in distributions and abundances across species, testing for the effects of changing environmental conditions and human-induced pressures that are expected to affect species distributions (Engelhard et al. 2014). In the North Sea, ecosystem regime shifts have been observed (Beaugrand 2004, Sguotti et al. 2022), as well as long-term changes in ambient sea temperatures that are affecting thermoregulatory processes (Perry et al. 2005, Sguotti et al. 2016). Strong human-induced pressures on rays that could be included in future studies include fishing effort from demersal fishing fleets where rays occur as bycatch (Walker and Hislop 1998). However, long-term spatially explicit time series for fishing effort are lacking for the study area. Other anthropogenic activities with the potential to lead to changes in spatial distribution through habitat alteration include shipping, aggregate extraction, oil and gas exploration, coastal developments, and wind farm constructions. INLA-SPDE models have already been used to study changes in bird populations in the context of offshore wind farm development (Vilela et al. 2021).

The temporal correlation in the spatial field was modelled with nine evenly spaced temporal knots across the years 1988–2023. This approach of using multi-year knots prevents prohibitively high computational costs of analysing spatio-temporal correlation compared to an approach where each year is treated as a single knot. Under the assumption that changes in the spatial distributions occur gradually, the multi-year knot approach should yield results that are comparable to having a higher resolution of knots. Estimates of the spatial field for individual years, between knots, require now interpolation, and may underestimate rates of changes in spatial distribution.

To conclude, we have used a size-structured model with spatio-temporal correlation to show how the thornback ray population in the greater North Sea ecoregion has increased in abundance recently. This increase was spatially heterogeneous and co-occurred with changes in the size distribution of the population. Further development of the INLA methodology (Rue et al. 2009) used here, achieving faster inference, improved numerical stability, and scalability (Van Niekerk et al. 2023), will allow expanding the application of INLA models within marine sciences and other fields to help gain new insights. The approach we followed could be applied to other data-limited stocks. But requires good research vessel survey data, including lengths of caught individuals. Ideally, these data are accompanied by estimates for gear efficiency derived from data-rich stocks for species with similar characteristics.

Author contributions

Timo Michael Staeudle: conceptualization, collection of data, data processing, model design, manuscript drafting and editing, revising manuscript. Jan Jaap Poos: conceptualization, model design, manuscript drafting and editing, revising manuscript. Bram Parmentier: conceptualization, model design, revising manuscript.

Supplementary data

Supplementary data is available at *ICES Journal of Marine Science* online.

Conflict of interest: The authors declare that they have no conflict of interest.

Data availability

The data underlying this article were derived from sources in the public domain:

- ICES database on trawl surveys (DATRAS; ICES 2023b): https://datras.ices.dk.
- EUSeaMap 2021 Broad-Scale Predictive Habitat Map for Europe (Vasquez et al. 2021); creation date: 23.09.2021; unique resource identifier: 5877d808-3fd7-11eb-b378-0242ac130002: https://emodnet.ec.europa.eu/geonetwork/srv/eng/catalog.search#/metadata/10d3d35c-8f8e-40ff-898f-32e0b037356c.
- Depth data were obtained from the European Marine Observation and Data Network (EMODnet) Bathymetry Portal: https://portal.emodnet-bathymetry.eu/.

The processed data and code used for analyses underlying this manuscript are publicly available at 4TU.ResearchData: https://doi.org/10.4121/aa23c8b5-5441-4ac9-9e02-808bbf6b872e

References

Aarts G, Poos JJ. Comprehensive discard reconstruction and abundance estimation using flexible selectivity functions. *ICES J Mar Sci* 2009;**66**:763–71. https://doi.org/10.1093/icesjms/fsp033

Alglave B, Rivot E, Etienne M-P *et al.* Combining scientific survey and commercial catch data to map fish distribution. *ICES J Mar Sci* 2022;**79**:1133–49. https://doi.org/10.1093/icesjms/fsac032

Amelot M, Batsleer J, Foucher E *et al.* Evidence of difference in landings and discards patterns in the English Channel and North Sea Rajidae complex fishery. *Fish Res* 2021;**242**:106028. https://doi.org/10.1016/j.fishres.2021.106028

Auber A, Ernande B, Travers-Trolet M *et al.* Intercalibration of research survey vessels: "GWEN DREZ" and "THALASSA. 2015.https://archimer.ifremer.fr/doc/00293/40417/

Bakka H, Rue H, Fuglstad GA *et al.* Spatial modeling with R-INLA: a review. *WIREs Comput Stat* 2018;**10**:e1443. https://doi.org/10.1002/wics.1443

Banerjee S. *Hierarchical Modeling and Analysis for Spatial Data*. Boca Raton, FL: Chapman & Hall/CRC Press, 2004.

Baum JK, Worm B. Cascading top-down effects of changing oceanic predator abundances. *J Anim Ecol* 2009;**78**:699–714. https://doi.org/10.1111/j.1365-2656.2009.01531.x

Beaugrand G. The North Sea regime shift: evidence, causes, mechanisms and consequences. *Prog Oceanogr* 2004;**60**:245–62. https://doi.org/10.1016/j.pocean.2004.02.018

Bellodi A, Carbonara P, MacKenzie KM *et al.* Measurement of the growth of the main commercial rays (*Raja clavata*, *Raja brachyura*, *Torpedo marmorata*, *Dipturus oxyrinchus*) in European waters using intercalibration methods. *Biology* 2024;**13**:20. https://doi.org/10.3390/biology13010020

Berg M, Cheong O, Kreveld M *et al.* *Computational Geometry: Algorithms and Applications*. New York: Springer Berlin, Heidelberg, 2008.

Blangiardo M, Cameletti M, Baio G *et al.* Spatial and spatio-temporal models with R-INLA. *Spat Spatio-temporal Epidemiol* 2013;**4**:33–49. https://doi.org/10.1016/j.sste.2012.12.001

Bogaards JA, Kraak SBM, Rijnsdorp AD. Bayesian survey-based assessment of North Sea plaice (*Pleuronectes platessa*): extracting integrated signals from multiple surveys. *ICES J Mar Sci* 2009;**66**:665–79. https://doi.org/10.1093/icesjms/fsp038

Chevolot M, Ellis JR, Hoarau G *et al.* Population structure of the thornback ray (*Raja clavata* L.) in British waters. *J Sea Res* 2006;**56**:305–16. https://doi.org/10.1016/j.seares.2006.05.005

Cook RM. Inclusion of discards in stock assessment models. *Fish Fish* 2019;**20**:1232–45. https://doi.org/10.1111/faf.12408

Dambly LI, Isaac NJB, Jones KE *et al.* Integrated species distribution models fitted in INLA are sensitive to mesh parameterisation. *Ecography* 2023;**2023**:e06391. https://doi.org/10.1111/ecog.06391

Dulvy NK, Baum JK, Clarke S *et al.* You can swim but you can't hide: the global status and conservation of oceanic pelagic sharks and rays. *Aquat Conserv: Mar Freshw Ecosyst* 2008;**18**:459–82. https://doi.org/10.1002/aqc.975

Dulvy NK, Simpfendorfer CA, Davidson LNK *et al.* Challenges and priorities in shark and ray conservation. *Curr Biol* 2017;**27**:R565–72. https://doi.org/10.1016/j.cub.2017.04.038

Ellis JR, Clarke MW, Corts E *et al.* Management of Elasmobranch Fisheries in the North Atlantic. In: A Payne, J Cotter, T Potter (eds), *Advances in Fisheries Science: 50 Years on From Berverton and Holt*. Oxford: Blackwell Publishing Ltd., 184–228, 2008.

Engelhard A. One hundred and twenty years of change in fishing power of English North Sea trawlers. In: A Payne, J Cotter, T Potter (eds), *Advances in Fisheries Science: 50 Years On from Berton and Holt*, Oxford: Blackwell Publishing, 2008, 1–25.

Engelhard GH, Lynam CP, García-Carreras B *et al.* Effort reduction and the large fish indicator: spatial trends reveal positive impacts of recent European fleet reduction schemes. *Environ Conserv* 2015;**42**:227–36. https://doi.org/10.1017/S0376892915000077

Engelhard GH, Righton DA, Pinnegar JK. Climate change and fishing: a century of shifting distribution in North Sea cod. *Global Change Biol* 2014;**20**:2473–83. https://doi.org/10.1111/gcb.12513

Fletcher RJ, Hefley TJ, Robertson EP *et al.* A practical guide for combining data to model species distributions. *Ecology* 2019;**100**:e02710. https://doi.org/10.1002/ecy.2710

Fournier DA, Doonan IJ. A length-based stock assessment method utilizing a generalized delay-difference model. *Can J Fish Aquat Sci* 1987;**44**:422–37. https://doi.org/10.1139/f87-051

Gallagher AJ, Kyne PM, Hammerschlag N. Ecological risk assessment and its application to elasmobranch conservation and management. *J Fish Biol* 2012;**80**:1727–48. https://doi.org/10.1111/j.1095-8649.2012.03235.x

Goethel DR, Cadrin SX. Revival and recent advancements in the spatial fishery models originally conceived by Sidney Holt and Ray Beverton. *ICES J Mar Sci* 2021;**78**:2298–315. https://doi.org/10.1093/icesjms/fsab021

Holden MJ. The fecundity of *Raja clavata* in British waters. *ICES J Mar Sci* 1975;**36**:110–8. https://doi.org/10.1093/icesjms/36.2.110

Hunter E, Berry F, Buckley AA *et al.* Seasonal migration of thornback rays and implications for closure management. *J Appl Ecol* 2006;**43**:710–20. https://doi.org/10.1111/j.1365-2664.2006.01194.x

Hunter E, Buckley AA, Stewart C *et al.* Migratory behaviour of the thornback ray, *Raja clavata*, in the southern North Sea. *J Mar Biol Assoc UK* 2005;**85**:1095–105. https://doi.org/10.1017/S0025315405012142

ICES. *Report of the Working Group on Elasmobranch Fishes (WGEF), 31 May–7 June 2017*. **16**, p. 1018, 2017. Lisbon, Protugal.

ICES. Thornback ray (*Raja clavata*) in Subarea 4 and in divisions 3.a and 7.d (North Sea, Skagerrak, Kattegat, and eastern English Channel). *In Report of the ICES Advisory Committee, 2021. ICES Advice 2021, rjc.27.3a47d*, 2021. http://doi.org/10.17895/ices.pub.22760042

ICES. Benchmark Workshop for selected elasmobranch stocks (WKBELASMO). *ICES Scientific Reports*, **5**:117 pp. 2023a. https://doi.org/10.17895/ices.pub.22760042

ICES. *ICES Database of Trawl Surveys (DATRAS)*. Copenhagen, Denmark: ICES, 2023b. https://datras.ices.dk

Jona Lasinio G, Mastrantonio G, Pollice A. Discussing the "big n problem". *Stat Methods Appl* 2013;**22**:97–112.

Kelleher K. *Discards in the World's Marine Fisheries: An Update*. Rome, Italy: FAO, 131pp, 2005.

Kraak SBM, Daan N, Pastoors MA. Biased stock assessment when using multiple, hardly overlapping, tuning series if fishing trends vary spatially. *ICES J Mar Sci* 2009;**66**:2272–7. https://doi.org/10.1093/icesjms/fsp179

Lezama-Ochoa N, Pennino MG, Hall MA *et al.* Using a Bayesian modelling approach (INLA-SPDE) to predict the occurrence of the Spinetail Devil Ray (*Mobular mobular*). *Sci Rep* 2020;**10**:18822. https://doi.org/10.1038/s41598-020-73879-3

Lindgren F, Rue H. Bayesian spatial modelling with R-INLA. *J Stat Softw* 2015;**63**: 1–25. https://doi.org/10.18637/jss.v063.i19

Lindgren F, Rue H, Lindström J. An explicit link between Gaussian fields and Gaussian Markov random fields: the stochastic partial differential equation approach. *J R Stat Soc Ser B: Stat Methodol* 2011;**73**:423–98. https://doi.org/10.1111/j.1467-9868.2011.00777.x

McCully SR, Scott F, Ellis JR. Lengths at maturity and conversion factors for skates (Rajidae) around the British Isles, with an analysis of data in the literature. *ICES J Mar Sci* 2012;**69**:1812–22. https://doi.org/10.1093/icesjms/fss150

McInturf AG, Bowman J, Schulte JM *et al.* A unified paradigm for defining elasmobranch aggregations. *ICES J Mar Sci* 2023;**80**:1551–66. https://doi.org/10.1093/icesjms/fsad099

Moriarty M, Sethi SA, Pedreschi D *et al.* Combining fisheries surveys to inform marine species distribution modelling. *ICES J Mar Sci* 2020;**77**:539–52. https://doi.org/10.1093/icesjms/fsz254

Musick JA, Burgess G, Cailliet G *et al.* Management of Sharks and Their Relatives (Elasmobranchii). *Fisheries* 2000;**25**:9–13. https://doi.org/10.1577/1548-8446(2000)025%3c0009:MOSATR%3e2.0.CO;2

Paradinas I, Conesa D, Pennino MG *et al.* Bayesian spatio-temporal approach to identifying fish nurseries by validating persistence areas. *Mar Ecol Prog Ser* 2015;**528**:245–55. https://doi.org/10.3354/meps11281

Paradinas I, Illian JB, Alonso-Fernández A *et al.* Combining fishery data through integrated species distribution models. *ICES J Mar Sci* 2023;**80**:2579–90. https://doi.org/10.1093/icesjms/fsad069

Paradinas I, Marín M, Grazia Pennino M *et al.* Identifying the best fishing-suitable areas under the new European discard ban. *ICES J Mar Sci* 2016;**73**:2479–87. https://doi.org/10.1093/icesjms/fsw114

Pedersen MW, Berg CW. A stochastic surplus production model in continuous time. *Fish Fish* 2017;**18**:226–43. https://doi.org/10.1111/faf.12174

Pennino MG, Conesa D, López-Quílez A *et al.* Fishery-dependent and -independent data lead to consistent estimations of essential habitats. *ICES J Mar Sci* 2016;**73**:2302–10. https://doi.org/10.1093/icesjms/fsw062

Pennino MG, Muñoz F, Conesa D *et al.* Modeling sensitive elasmobranch habitats. *J Sea Res* 2013;**83**:209–18. https://doi.org/10.1016/j.seares.2013.03.005

Perry AL, Low PJ, Ellis JR *et al.* Climate change and distribution shifts in marine fishes. *Science* 2005;**308**:1912–5. https://doi.org/10.1126/science.1111322

Pinto C, Travers-Trolet M, Macdonald JI *et al.* Combining multiple data sets to unravel the spatiotemporal dynamics of a data-limited fish stock. *Can J Fish Aquat Sci* 2019;**76**:1338–49. https://doi.org/10.1139/cjfas-2018-0149

R Core Team. *R: A Language and Environment for Statistical Computing*. Vienna, Austria: R Foundation for Statistical Computing, 2024. https://www.R-project.org/

Righetto AJ, Faes C, Vandendijck Y *et al.* On the choice of the mesh for the analysis of geostatistical data using R-INLA. *Commun Stat—Theory Methods* 2020;**49**:203–20. https://doi.org/10.1080/03610926.2018.1536209

Roos M, Held L. Sensitivity analysis in Bayesian generalized linear mixed models for binary data. *Bayes Anal* 2011;**6**:259–78. https://doi.org/10.1214/11-BA609

Rousset J. Population structure of thornback rays *Raja clavata* and their movements in the Bay of Douarnenez. *J Mar Biol Assoc UK* 1990;**70**:261–8. https://doi.org/10.1017/S0025315400035384

Rue H, Martino S, Chopin N. Approximate Bayesian inference for latent Gaussian models by using integrated nested Laplace approximations. *J R Stat Soc Ser B: Stat Methodol* 2009;**71**:319–92. https://doi.org/10.1111/j.1467-9868.2008.00700.x

Sadykova D, Scott BE, De Dominicis M *et al.* Bayesian joint models with INLA exploring marine mobile predator-prey and competitor species habitat overlap. *Ecol Evol* 2017;**7**:5212–26.

Sampson DB. Fishery selection and its relevance to stock assessment and fishery management. *Fish Res* 2014;**158**:5–14. https://doi.org/10.1016/j.fishres.2013.10.004

Santos R, Medeiros-Leal W, Novoa-Pabon A *et al.* Biological knowledge of thornback ray (*Raja clavata*) from the Azores: improving scientific information for the effectiveness of species-specific management measures. *Biology* 2021;**10**:676. https://doi.org/10.3390/biology10070676

Sguotti C, Blöcker AM, Färber L *et al.* Irreversibility of regime shifts in the North Sea. *Front Mar Sci* 2022;**9**:1–13.https://doi.org/10.3389/fmars.2022.945204

Sguotti C, Lynam CP, Garcia-Carreras B *et al.* Distribution of skates and sharks in the North Sea: 112 years of change. *Global Change Biol* 2016;**22**:2729–43. https://doi.org/10.1111/gcb.13316

Sherman CS, Sant G, Simpfendorfer CA *et al.* M-Risk: a framework for assessing global fisheries management efficacy of sharks, rays and chimaeras. *Fish Fish* 2022;**23**:1383–99. https://doi.org/10.1111/faf.12695

Stein RW, Mull CG, Kuhn TS *et al.* Global priorities for conserving the evolutionary history of sharks, rays and chimaeras. *Nat Ecol Evol* 2018;**2**:288–98.

Stevens JD, Bonfil R, Dulvy NK *et al.* The effects of fishing on sharks, rays, and chimaeras (chondrichthyans), and the implications for marine ecosystems. *ICES J Mar Sci* 2000;**57**:476–94. https://doi.org/10.1006/jmsc.2000.0724

Thorson JT, Cunningham CJ, Jorgensen E *et al.* The surprising sensitivity of index scale to delta-model assumptions: recommendations for model-based index standardization. *Fish Res* 2021;**233**:105745. https://doi.org/10.1016/j.fishres.2020.105745

Thorson JT, Minto C. Mixed effects: a unifying framework for statistical modelling in fisheries biology. *ICES J Mar Sci* 2015;**72**:1245–56. https://doi.org/10.1093/icesjms/fsu213

Thys KJM, Lemey L, Van Bogaert N. Blondes do it better? A comparative study on the morphometry and life-history traits of commercially important skates blonde ray *Raja brachyura*, thornback ray *Raja clavata*, and spotted ray *Raja montagui*, with management implications. *Fish Res* 2023;**263**:106679. https://doi.org/10.1016/j.fishres.2023.106679

Van Niekerk J, Krainski E, Rustand D *et al.* A new avenue for Bayesian inference with INLA. *Comput Stat Data Anal* 2023;**181**:107692. https://doi.org/10.1016/j.csda.2023.107692

Vasquez M, Allen H, Manca E *et al.* EUSeaMap 2021. A European broad-scale seabed habitat map. Ref. D1.13 EASME/EMFF/2018/1.3.1.8/Lot2/SI2.810241– EMODnet Thematic Lot n° 2–Seabed Habitats EUSeaMap 2021–Technical Report. EMODnet. 2021. https://doi.org/10.13155/83528

Vilela R, Burger C, Diederichs A *et al.* Use of an INLA latent Gaussian modeling approach to assess bird population changes due to the development of offshore wind farms. *Front Mar Sci* 2021;**8**:1–11. https://doi.org/10.3389/fmars.2021.701332

Walker ND, Maxwell DL, Le Quesne WJF *et al.* Estimating efficiency of survey and commercial trawl gears from comparisons of catch-ratios. *ICES J Mar Sci* 2017;**74**:1448–57. https://doi.org/10.1093/icesjms/fsw250

Walker P, Howlett G, Millner R. Distribution, movement and stock structure of three ray species in the North Sea and eastern English Channel. *ICES J Mar Sci* 1997;**54**:797–808. https://doi.org/10.1006/jmsc.1997.0223

Walker PA. *Fleeting Images: Dynamics of North Sea Ray Populations*. Amsterdam: University of Amsterdam, 1999.

Walker PA, Heessen HJL. Long-term changes in ray populations in the North Sea. *ICES J Mar Sci* 1996;**53**:1085–93. https://doi.org/10.1006/jmsc.1996.0135

Walker PA, Hislop JRG. Sensitive skates or resilient rays? Spatial and temporal shifts in ray species composition in the central and north-western North Sea between 1930 and the present day. *ICES J Mar Sci* 1998;**55**:392–402. https://doi.org/10.1006/jmsc.1997.0325

Winker H, Carvalho F, Kapur M. JABBA: just another Bayesian biomass assessment. *Fish Res* 2018;**204**:275–88. https://doi.org/10.1016/j.fishres.2018.03.010

Worm B, Orofino S, Burns ES *et al*. Global shark fishing mortality still rising despite widespread regulatory change. *Science* 2024;**383**:225–30. https://doi.org/10.1126/science.adf8984

Wright SR, Lynam CP, Righton DA *et al*. Structure in a sea of sand: fish abundance in relation to man-made structures in the North Sea. *ICES J Mar Sci* 2020;**77**:1206–18. https://doi.org/10.1093/icesjms/fsy142

Zuur AF, Ieno EN, Saveliev AA. *Beginner's Guide to Spatial, Temporal, and Spatial-Temporal Ecological Data Analysis with R-INLA*. Newburgh, Scotland: Highland Statistics Ltd. 2017.

Handling Editor: Stan Kotwicki